applied optics

# Graphics processing unit–assisted real-time three-dimensional measurement using speckle-embedded fringe

Shijie Feng,[1,*] Qian Chen,[1,2] and Chao Zuo[1,3]

[1]Jiangsu Key Laboratory of Spectral Imaging & Intelligent Sense, Nanjing University of Science and Technology, Nanjing, Jiangsu Province 210094, China
[2]e-mail: chenqian@njust.edu.cn
[3]e-mail: surpasszuo@163.com
*Corresponding author: geniusshijie@163.com

Received 26 May 2015; revised 7 July 2015; accepted 7 July 2015; posted 7 July 2015 (Doc. ID 241379); published 29 July 2015

**This paper presents a novel two-frame fringe projection technique for real-time, accurate, and unambiguous three-dimensional (3D) measurement. One of the frames is a digital speckle pattern, and the other one is a composite image which is generated by fusing that speckle image with sinusoidal fringes. The contained sinusoidal component is used to obtain a wrapped phase map by Fourier transform profilometry, and the speckle image helps determine the fringe order for phase unwrapping. Compared with traditional methods, the proposed pattern scheme enables measurements of discontinuous surfaces with only two frames, greatly reducing the number of required patterns and thus reducing the sensitivity to movements. This merit makes the method very suitable for inspecting dynamic scenes. Moreover, it shows close performance in measurement accuracy compared with the phase-shifting method from our experiments. To process data in real time, a Compute Unified Device Architecture–enabled graphics processing unit is adopted to accelerate some time-consuming computations. With our system, measurements can be performed at 21 frames per second with a resolution of 307,000 points per frame.** 

***OCIS codes:*** (100.5070) Phase retrieval; (150.6910) Three-dimensional sensing; (110.6880) Three-dimensional image acquisition; (120.5050) Phase measurement; (120.3940) Metrology.

http://dx.doi.org/10.1364/AO.54.006865

## 1. INTRODUCTION

Three-dimensional (3D) surface measurement is playing a significant role in both scientific and industrial areas [1,2]. Compared with traditional methods, such as the coordinate measuring machine retrieving a 3D contour by pointwise physical contact, optics-based 3D profilometry offers noncontact and flexible measurement. Various optical approaches have been developed, including fringe projection profilometry (FPP), stereo vision, time-of-flight techniques, Moiré contouring, and so on [3–6]. Among them, FPP is one of the most reliable techniques for recovering the profile due to its superiorities of full-field measurement, high accuracy, and pixel-level resolution. Recently, with advances in digital light projection devices, high-speed, real-time 3D measurements based on FPP are expanding rapidly [7–11]. This kind of measurement enables a quick investigation of tested scenes, making the 3D reconstruction results able to be viewed and analyzed in an interactive manner. Thus it would show great significance in various fields such as medical imaging, virtual reality, industrial manufacturing, and computer vision [12,13]. However, for fast, real-time FPP, there are two main challenges facing researchers. The first one is how to efficiently, accurately, and unambiguously recover the phase information [14,15]. As conventional FPP techniques are developed to inspect static objects in a non-time-critical condition [12], they usually have difficulties in measuring dynamic scenes because it is difficult for them to obtain the shape within an extremely short period of time (e.g., tens of milliseconds or less). Then the next challenge is to improve the data processing speed [16]. This is because the calculations of the phase and the 3D coordinates are very complex. A favorable computational speed can guarantee the desired real-time performance for the measurement.

To deal with the first challenge, some researchers resort to Fourier transform profilometry (FTP), by which only a single fringe pattern is sufficient to retrieve the phase [17–20]. This technique is particularly suitable for high-speed measurement because of its high efficiency. However, when a surface with largely varying slope is tested, the frequency overlapping

problem may emerge, which makes this frequency-domain-filtering-based technique suffer [18]. Although this problem could be remedied by a $\pi$ phase-shifting FTP [21], the demand for an additional pattern would influence the instantaneous feature of the FTP to some extent. Besides, to unambiguously unwrap the phase for absolute depth recovery, temporal phase unwrapping methods are commonly adopted [22–26]. However, one should carefully design the frequencies of the patterns and control the noise. Generally, it is recommended for FTP to analyze a high-frequency fringe pattern since this will facilitate the extraction of the first order term of the spectrum as the first order term would overlap with the fundamental frequency easily if the frequency is not high enough. But as the frequency gets higher, the phase unwrapping for temporal methods would become more difficult due to the effect of the random noise [27,28]. Therefore, different patterns with more than two frequencies are usually used to alleviate this influence in temporal phase unwrapping. In [29], a dynamic object was measured with fringes of three different frequencies. On the other hand, other researchers adopt phase-shifting profilometry (PSP) to achieve high-speed 3D measurement. PSP has the advantages of higher accuracy and resolution and greater insensitivity to ambient light compared with FTP. Wang and Zhang [30] proposed a method using nine patterns to conduct high-speed measurements. Then, to reduce the number of required patterns, Liu *et al.* [31] presented a dual-frequency pattern scheme where a high-frequency component is used to generate robust phase information, and a unit-frequency component is used to eliminate the phase ambiguity. The method can achieve a phase map of high quality with five patterns. Next, Zuo *et al.* proposed a four-frame pattern projection strategy, which is composed of two frames of sinusoidal fringes and two linearly varying gray-scale images. With their system, a measurement speed of 120 frames per second (FPS) is achieved [28]. To further increase the measurement speed, binary pattern projection strategies were developed to rapidly project fringe images using a defocused projector [32–34]. For PSP, the minimum step of the phase shift is three; thus the three-step phase-shifting method is usually adopted to reconstruct a 3D shape in time-critical situations. Zhang *et al.* introduced a speckle image into the three-step phase-shifting algorithm to present a speckle-embedded fringe projection method [35]. The sinusoidal fringes are used to retrieve the phase information, and the embedded speckle is used to determine the fringe order of each stripe. As a result, the absolute depth can be retrieved with three patterns. It can be seen that although the PSP methods have favorable advantages, at least three fringe images are required for them to achieve 3D reconstruction, which still shows relatively high sensitivity to movement.

Several efforts have also been made to cope with the second challenge of boosting the data processing speed for 3D shape reconstruction. For PSP techniques, Zhang *et al.* used a graphics processing unit (GPU) to accelerate the procedures of coordinate acquisition, 3D reconstruction, and display, achieving a measurement speed of 30 FPS [36]. Liu *et al.* employed a lookup table to bypass the time-consuming computation of the arctangent for the phase calculation [31]. Their measurement speed, thus, is greatly improved to 228 FPS. Recently, Nguyen *et al.* developed a real-time 3D measurement system which relied on the multithread computing of the central processing unit (CPU), allowing absolute depth measurements at 22.5 FPS [37]. For FTP techniques, as the Fourier transform is extremely time-consuming, to our knowledge few works have been reported to achieve real-time measurements. A common strategy for FTP to inspect a moving object is to record and save the dynamic process in advance and carry out the fringe analysis for 3D reconstruction offline.

In this paper, we propose a novel two-frame, speckle-embedded fringe projection method to handle these challenges. One of the patterns is the speckle image, and the other is a composite fringe pattern which is composed of that speckle image and sinusoidal fringes. Through a subtraction of these two images, we can obtain the contained sinusoidal component, which is then used to retrieve the phase through FTP. Note that in the pattern design we add a DC component to the speckle image; thus the subtraction will eliminate the fundamental frequency component of the resultant sinusoidal image. Then, to unwrap the solved phase unambiguously, the idea of digital speckle temporal sequence correlation is introduced [38]. To accelerate the data processing speed, a GPU with Compute Unified Device Architecture (CUDA) parallel computing is employed. The processes of phase computation, speckle correlation, phase unwrapping, and 3D reconstruction are all carried out in the GPU. Compared with conventional approaches, the method has several distinct merits. First, it only requires two patterns to conduct 3D reconstructions. The technique takes advantage of the single-frame characteristic of FTP. Combined with the strategy of removing the fundamental frequency, the method also improves the precision of FTP. Second, it makes use of the locally unique distribution of the speckle signal to unwrap the phase, removing the phase ambiguity by only one additional pattern. Last, to the best of our knowledge, it is the first work to carry out FTP in a real-time manner. Our experiments show that the performance of our method is very close to that of the conventional methods in term of measurement accuracy, which indicates it has met the demand for real-time measurement. With our system, it is able to measure moving objects at 21 FPS with a resolution of 307,000 points per frame.

## 2. PRINCIPLES

### A. Pattern Design

To present a method less sensitive to movement, we adopt FTP as it is capable of retrieving the phase information from a single fringe pattern. Then, to unwrap the phase without introducing too many assistant patterns, in [35] we find a digital speckle image can help determine the fringe order for the wrapped phase. Thus, we introduce a speckle pattern into our method for full-field, unambiguous phase unwrapping. Moreover, to bypass the frequency overlapping problem, the speckle image is embedded into the fringe pattern. By the subtraction of these two images, a pure sinusoidal fringe without the fundamental frequency will be obtained. The speckle image is expressed by

$$I_{\mathrm{spe}}(x,y) = AS(x,y) + \frac{A}{2}, \tag{1}$$

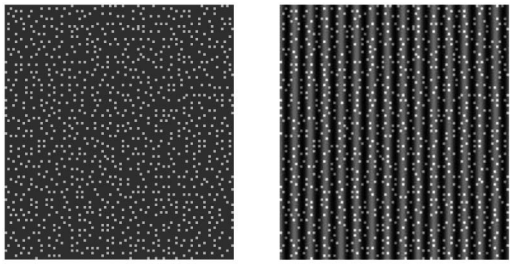

(a) (b)

**Fig. 1.** Two generated patterns. (a) Speckle image; (b) Speckle-embedded fringe.

where $S(x, y) \in \{0, 1\}$ depicts the distribution of the speckle, $A$ controls its intensity, and $A/2$ is the DC component. For image pixels with $N$ bits gray level, $A$ equals $2^{N-2}$. To make the speckle $S(x, y)$ be of high distinguishability, it is designed based on the following rules [35]: (1) The speckle is simulated by white dots randomly distributed on a black background, and the size of each white dot is $M \times M$ pixels; (2) in each area with equivalent size of $3 \times 3$ dots, only one dot is white; (3) no two white dots are adjacent in their eight neighborhoods. Figure 1(a) shows the generated speckle image $I_{\text{spe}}$. Then a sinusoidal fringe is fused with the speckle pattern, which can be written as

$$I_{\text{sin\_spe}}(x, y) = I_{\text{spe}}(x, y) + B \cos(2\pi f x), \tag{2}$$

where $f$ is the frequency of the sinusoidal component and $B$ its intensity modulation, which is equal to $A/2$. Figure 1(b) shows the simulated speckle-embedded fringe pattern.

### B. Phase Retrieval

The typical arrangement of a fringe projection system is shown in Fig. 2. A set of fringe patterns is projected onto a measured object, and the images of the patterns distorted by the object surface are captured by a camera from a different angle. For the proposed method, the captured images can be expressed by

$$I^c_{\text{spe}}(x, y) = \alpha(x, y) I_{\text{spe}}(x, y) + \beta(x, y), \tag{3}$$

$$I^c_{\text{sin\_spe}}(x, y) = \alpha(x, y) I_{\text{sin\_spe}}(x, y) + \beta(x, y), \tag{4}$$

where $I^c_{\text{spe}}$ and $I^c_{\text{sin\_spe}}$ are the captured speckle image and speck-embedded sinusoidal image, respectively; $\alpha$ and $\beta$ are

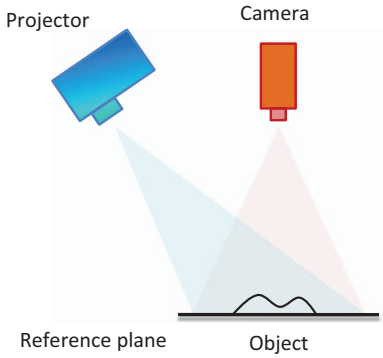


**Fig. 2.** Typical arrangement of a fringe projection system.

the reflectivity of the object and the captured ambient light, respectively. To obtain the contained sinusoidal component, Eq. (3) is subtracted from Eq. (4), giving a speckle-free fringe pattern $I_{\text{fringe}}$:

$$I_{\text{fringe}}(x, y) = \alpha(x, y) B \cos \phi(x, y), \tag{5}$$

where $\phi(x, y)$ is the phase to be solved. In FTP, the fringe pattern can be written as a Fourier series expansion:

$$I_{\text{fringe}}(x, y) = \sum_{n=-\infty}^{+\infty} A_n r(x, y) \exp[\text{in}\phi(x, y)]. \tag{6}$$

As the gamma distortion of projector will introduce undesired high-frequency components to the Fourier spectra of the captured fringe pattern, the method reported in [28] can be applied to eliminate its impact. After applying the 2D Fourier transform to the fringe image, we employ a 2D Hanning filter to extract the first order term of the Fourier spectra since it is able to reinforce the frequencies near the carrier frequency and attenuate the rest as the distance to the carrier frequency is increased [18]. Moreover, the ringing effect (Gibbs phenomenon) can also be effectively suppressed due to the smooth frequency response. The frequency response function of the filter is written as

$$H(f_x, f_y) = \frac{1}{4}\left[1 + \cos\left(\varepsilon\pi \frac{f_x - f_0}{f_{cx}}\right)\right]\left[1 + \cos\left(\varepsilon\pi \frac{f_y}{f_{cy}}\right)\right], \tag{7}$$

where $f_0$ is the frequency of the observed fringe, $(f_{cx}, f_{cy})$ is the cutoff frequency at 50% attenuation ratio, and $\varepsilon$ equals 0.5. Then the inverse 2D Fourier transform is applied, giving

$$I_F = A_1 r(x, y) \exp[i\phi(x, y)]. \tag{8}$$

We can find that since the DC component $A/2$ is added to the speckle pattern, the subtraction eliminates the background intensity of the sinusoidal fringe as shown in Eq. (5). This means there will exist no zero order component in its Fourier spectra, solving the problem of frequency overlapping. With Eq. (8), the phase $\phi(x, y)$ can be calculated by

$$\phi(x, y) = \arctan \frac{\text{Im}[I_F(x, y)]}{\text{Re}[I_F(x, y)]}, \tag{9}$$

$$\Phi(x, y) = \phi(x, y) + 2\pi N(x, y), \tag{10}$$

where $N(x, y)$ is the fringe order and $\Phi(x, y)$ the unwrapped phase. It can be seen that the phase $\phi(x, y)$ solved from the arctan function is actually a principal value ranging from $-\pi$ to $+\pi$, having discontinuities with $2\pi$ phase jumps. Thus a phase unwrapping algorithm is always needed to remove the phase ambiguity. Generally, the spatial phase unwrapping methods are employed in FTP. These approaches are designed relying on the phase relationship between spatially adjacent pixels. They have a tendency to fail in areas around discontinuities in depth such as steps or holes because it is difficult for them to identify the number of phase jumps of $2\pi$ correctly in those regions. As the spatial phase unwrapping has limitations in unwrapping the phase of a surface with abrupt depth variation, temporal phase unwrapping is developed with the idea of introducing intermediate phase information to remove the

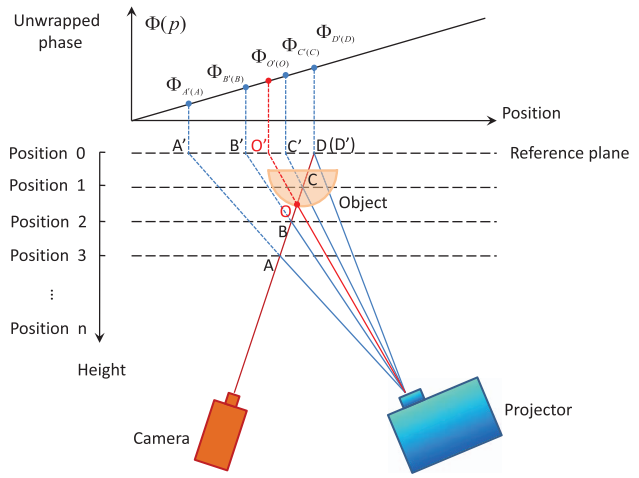


**Fig. 3.** Schematic of the identification for the fringe order.

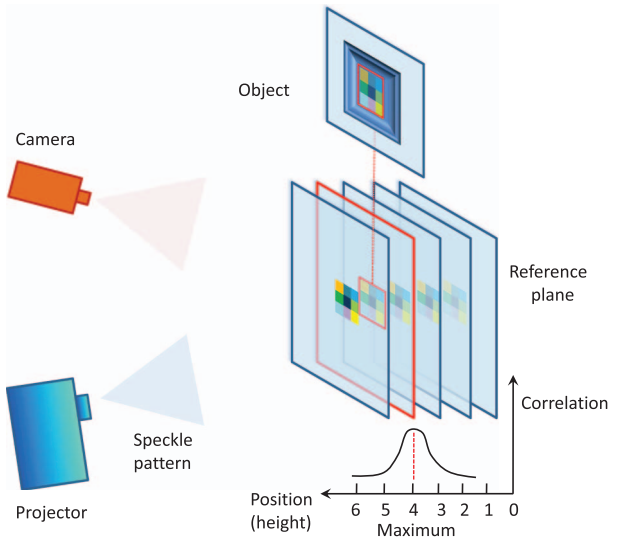


**Fig. 4.** Schematic of the height estimation using the correlation of speckle images.

depth ambiguities. It can be seen that the phase unwrapping is achieved with the sacrifice of an increased number of used patterns, so it may be inappropriate for the temporal unwrapping method to be applied to fast, real-time measurements. Here, in order to remove the phase ambiguity with fewer patterns, we take advantage of the speckle image.

From Eq. (10), we find that as the wrapped phase $\phi(x, y)$ is solved, the fringe order $N(x, y)$ can be determined if the unwrapped phase $\Phi(x, y)$ could be calculated. Thus, the speckle image is introduced to estimate the unwrapped phase map. To be specific, the unwrapped phase will be computed by a polynomial fitting which will be detailed later. The fitted phase may not be of very high precision. But it can be used for the identification of the fringe order. The method is illustrated as follows, and Fig. 3 shows the schematic. A series of patterns involving the speckle image $I_{\text{spe}}$, the speckle-embedded fringe image $I_{\text{sin\_spe}}$, and images $I_1$–$I_n$ are first generated by computer, where $I_1$–$I_n$ are phase-shifting fringes with different frequencies. Then all of these patterns are projected onto a reference plane by a projector and captured by a camera. The reference plane will be moving along the direction of height with equal steps; thus we can capture a set of speckle images $S(p)$, a set of speckle-embedded fringes $E(p)$, and a set of phase-shifting fringes $F(p)$ at different heights, where $p$ indicates the position (height) of the reference plane. At each height, with $F(p)$ several wrapped phase maps can be acquired using the phase-shifting method, and then an unwrapped phase map can be obtained by a temporal phase unwrapping method if the frequencies of the phase-shifting images $I_1$–$I_n$ are properly designed.

In Fig. 3, from the view of the camera, points $A$, $B$, $C$, and $D$ are located at different reference planes but will be captured by the same pixel. From the view of the projector, it is not hard to find that $\Phi_{A'} = \Phi_A$, $\Phi_{B'} = \Phi_B$, $\Phi_{C'} = \Phi_C$, and $\Phi_{D'} = \Phi_D$, where points $A'$, $B'$, $C'$, and $D'$ are the projections of points $A$, $B$, $C$, and $D$ on the reference plane at position 0. When the projected fringe is vertical, in the horizontal direction the phase values of points $A'$, $B'$, $C'$, and $D'$ will be distributed on a monotonically increasing (or decreasing) curve. Thus for the pixel, the unwrapped phases $\Phi_A$, $\Phi_B$, $\Phi_C$, and $\Phi_D$ will also be distributed in the same way. The upper half of Fig. 3 shows the relation between the position of the reference plane and its corresponding unwrapped phase for the pixel. When the reference plane is replaced by an object to be tested, the unwrapped phase of the measured point $O$ will also locate on the same curve. To build the relation between the position and the unwrapped phase, the polynomial fitting is employed since the positions are known at each depth and their corresponding unwrapped phases can be solved with phase-shifting images $I_1$–$I_n$. Thus by the polynomial fitting an approximate unwrapped phase of point $O$ can be acquired once its position is known.

In order to estimate the position of point $O$, we introduce the method presented in [38]. The schematic is shown in Fig. 4. For each reference plane at a different height, a speckle image is captured. Once the reference plane is replaced by the object, the measured point will have the same height as one of the reference planes does if they share nearly the same speckle from a subimage, except that the former may be partly deformed by the object's shape. Thus, the correlation between them is maximal. The correlation can be carried out by

$$\text{corr} = \frac{\sum_{x,y}(Q(x,y) - \bar{Q})(R(x,y) - \bar{R})}{\sqrt{\sum_{x,y}(Q(x,y) - \bar{Q})^2}\sqrt{\sum_{x,y}(R(x,y) - \bar{R})^2}}, \tag{11}$$

where $Q$ is the subimage from the speckle image captured with the object and $R$ the one from the speckle image captured at a reference plane. $\bar{Q}$ and $\bar{R}$ denote the average intensity of $Q$ and $R$, respectively. It is not difficult to find that this process may be very time-consuming if the object speckle image is to be correlated with all of the reference speckle images. Thus to tackle the issue, we resort to the obtained wrapped phase. We find that when the height of the object is equal to that of a reference plane, their subimages share not only similar speckle patterns but also the same wrapped phase. Therefore, we first compare the wrapped phase of the object with those of the reference

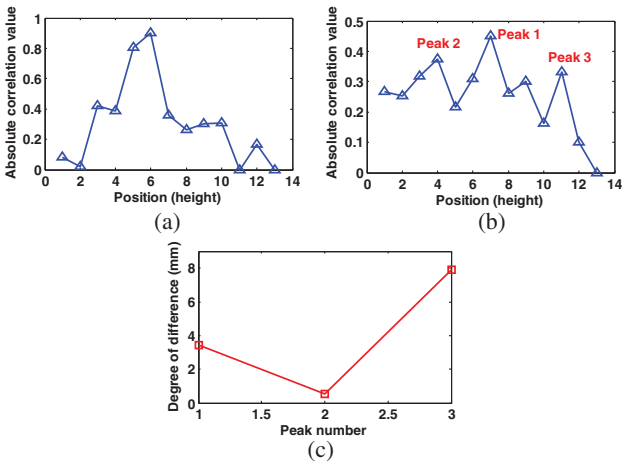


**Fig. 5.** Correlation curves and correction of erroneous height. (a) Typical curve with a main peak; (b) curve with multiple peaks when complex surface is inspected; (c) degree of difference for the peaks shown in (b).

planes. If a reference plane has a similar wrapped phase, its speckle pattern will be preserved as a candidate for the subsequent speckle image correlation. In this way, the computational time for the correlation is saved. Then to precisely determine the position, a curve-fitting algorithm called the center of gravity is applied. A total of $2\nu + 1$ points around the peak of the correlation curve will be used for the fit, and the precise position of pixel $(x, y)$ can be computed by

$$p(x,y) = \frac{\sum_{i=-\nu}^{\nu} \text{correlation}(p_0 + i)(p_0 + i)}{\sum_{i=-\nu}^{\nu} \text{correlation}(p_0 + i)}, \tag{12}$$

where $p_0$ is the position of the reference plane with the maximum correlation value.

As a more precise position is obtained, the unwrapped phase can be calculated by the polynomial fitting. As aforementioned, the estimated unwrapped phase is an approximate value; it cannot be used as the measurement result. But we are able to employ it to determine its corresponding fringe order, since the small difference between the approximate phase and the real one will not influence the identification of the fringe order. Thus, combined with the wrapped phase, the fringe order can be accurately retrieved by Eq. (10). Finally, again through Eq. (10) an accurate unwrapped phase can be recovered. In general, when the measured surface is of smooth shape, the correlation curve will have only a single peak as shown in Fig. 5(a). However, if the shape is partly complicated, a multi-peak correlation curve may be obtained for some pixels as shown in Fig. 5(b). In this case, the correlation values of the peaks are not high. The position with the maximum correlation value may not be the actual height, which may be indicated by the second peak, the third one, or so on. Thus, to handle this issue, we use a multiple-correlation-peak correction algorithm to correct erroneous heights:

$$D_j(x,y) = \text{abs}\{p_j(x,y) - \text{median}[NB(x,y)]\}, \tag{13}$$

where $D$ is the degree of difference, $j$ the $j$th highest peak of the correlation curve, $p_j$ the position indicated by the $j$th peak, and $NB$ the neighborhood of the pixel $(x, y)$ with size $s \times s$ in the position map solved with the first highest peak of the correlation curve. The function abs$(\cdot)$ means to calculate the absolute value, and $D_1$ is the difference between the height indicated by the highest correlation peak and its surrounding median height. The rule is that if the relation $D_t(x,y) = \min(D_j(x,y)) < D_1(x,y)$ holds for the $t$th highest peak, the position indicated by this peak is the true position to be solved. Figure 5(c) shows the degree of difference for the three peaks in Fig. 5(b). We can find that although the highest summit, Peak 1, has the largest correlation value, it still shows a relatively large height difference between the positions indicated by it and its neighboring points. Therefore, this highest peak may not be the one corresponding to the actual height. After inspecting the remaining peaks, we find that Peak 2, which is the second highest peak, has the smallest degree of difference. Thus, according to the criterion, Peak 2 is the desired peak indicating the actual position. For correction, the height indicated by Peak 2 is used to replace the erroneous height solved by the highest peak.

### C. Phase–Height Conversion

To convert the unwrapped phase to height accurately, we introduce a nonlinear phase-to-height mapping method based on a reference plane [39]. The height $z(x, y)$ is retrieved by the following relation:

$$\frac{1}{z(x,y)} = b_0(x,y) + \frac{b_1(x,y)}{\Delta\Phi(x,y)} + \frac{b_2(x,y)}{\Delta\Phi^2(x,y)} + \ldots + \frac{b_5(x,y)}{\Delta\Phi^5(x,y)}, \tag{14}$$

where $\Delta\Phi(x, y)$ is the relative absolute phase between the object and a fixed reference plane (e.g., $z = 0$). $b_0(x, y)$ to $b_5(x, y)$ are coefficients which can be readily solved by a least-square method since the height and its corresponding phase map for each reference plane can be obtained as in Section 2.B.

## 3. FLOW CHARTS OF THE PROPOSED METHOD

For better comprehension and implementation of our method, Fig. 6 summarizes the procedures of the method. Figure 6(a) describes the required preparation prior to the real-time measurement, and Fig. 6(b) illustrates the flowchart of the approach during the real-time process.

## 4. GPU-AIDED FAST DATA PROCESSING

To accelerate the computational speed of the method, we employ a GPU to assist with the fringe analysis and 3D reconstruction. Modern GPUs are very efficient at manipulating computer graphics and image processing, and their highly parallel structure makes them more effective than general-purpose CPUs for algorithms where processing large blocks of data is done in parallel. In this work, our programming is based on CUDA, which is a parallel computing platform and programming model created by NVIDIA and implemented by GPU. Figure 7 shows the details of the data processing carried out in the host personal computer and the GPU. At the very beginning of the real-time measurement, all of the data saved

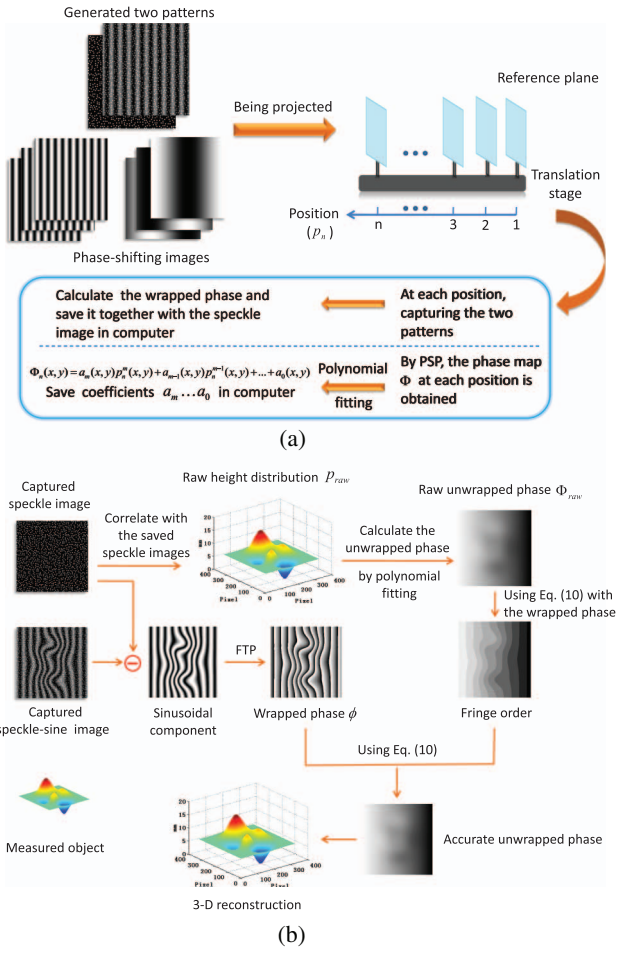


**Fig. 6.** (a) Preparation before the real-time measurement; (b) flowchart of the proposed method during the real-time process.

in preparatory work are first transferred from the host computer's memory to the global memory of the GPU. This step will only be performed once since the data are constant during the real-time procedure. Then the speckle image and the speckle-embedded pattern are captured and sent to the GPU's global memory where the image subtraction and phase computation through FTP are implemented by CUDA cores. After that, the solved wrapped phase together with the speckle image and the sets of wrapped phase and speckle images of the reference planes are all copied to the shared memory to perform the image correlation, raw height calculation, and correction. Then the solved height is transferred back to the global memory to solve the raw unwrapped phase and the fringe order. Last, the phase is accurately unwrapped and converted to height by the GPU. The 3D reconstruction is then transferred to the host and displayed with OpenGL (Open Graphics Library). For the calculations conducted in the GPU, we have the correlation and correction carried out in the shared memory. This is because the time of reading data from the shared memory is much less than that from the global memory. This optimized usage of the memory resources helps improve the computational efficiency significantly. However, for other procedures, the data are processed in global memory since the number

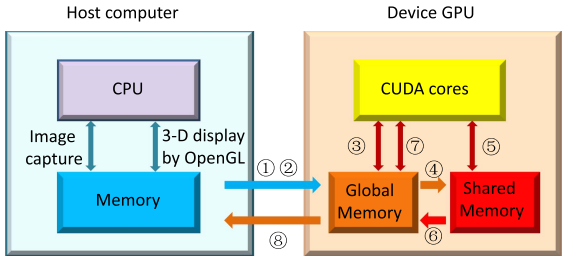


① : Data obtained in preparation are transferred to the global memory.
② : Sending the captured two patterns to GPU.
③ : Image subtraction and FTP.
④ : Transferring the solved wrapped phase together with captured speckle image and the sets of wrapped phase and speckle image of the reference planes to shared memory.
⑤ : Correlation of speckle image, raw height calculation and correction.
⑥ : Transferring the solved height back to global memory.
⑦ : Raw phase computation, fringe order determination, phase unwrapping and phase-height conversion.
⑧ : Transferring the 3-D reconstruction to host computer for display.

**Fig. 7.** Data processing procedures in the host PC and the GPU.

of reads is not large in these computations. In addition, to implement the Fourier transform rapidly, we employ a 2D Fourier transform function from the CUDA Fast Fourier Transform library, which further shortens the computational time of our method.

## 5. EXPERIMENTS

To test the validity of the proposed method, we established a real-time fringe projection system. It is composed of a high-speed CCD camera (AVT GE680) with resolution of 640 × 480, a digital light processing (DLP) Light Crafter with 608 × 684 resolution, and a desktop computer. The DLP Light Crafter does not have gamma distortion; thus no gamma correction algorithm is applied to the experiments. The Light Crafter sends trigger signals to the camera for image capture and synchronization. The photographed images are then processed in the computer. The computer used is a DELL ALWX51R with an Intel i7-4790 CPU and a NVidia GeForce GTX 760Ti graphics card. The graphics card has 1344 CUDA cores and 2 GB memory with a maximum bandwidth of 192.2 GB/sec. The two patterns are designed by Eq. (1) and Eq. (2). The frequency of the sinusoidal component is 100 cycles per field of view of 608 pixels.

In preparation, our measuring system translated 70 mm in a step of 1 mm on an electric control translation stage with a precision of 1 μm. The experimental setup is shown in Fig. 8(a). At each position, we projected and captured the speckle image, the speckle-embedded fringe, and three sets of three-step phase-shifting fringes with frequencies of 1, 10, and 100 cycles across the projection width. The speckle image and the solved wrapped phase map for each plane were saved for the following real-time measurement. With the phase-shifting images, the phase map at each height was calculated by the three-step phase-shifting algorithm and unwrapped by the multifrequency phase unwrapping method. Then the relation between the height and the unwrapped phase was fitted by a fourth order polynomial. This relation was also stored in the

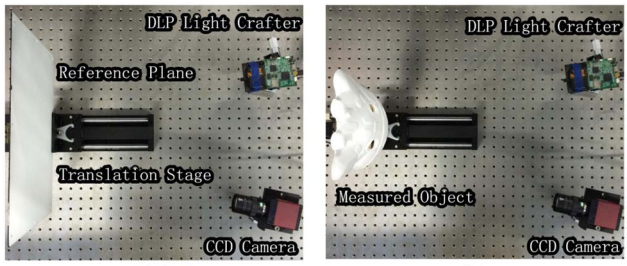


**Fig. 8.** (a) Experimental setup for the preparation; (b) image of the measurement of a cartoon face.

computer in advance for the calculation of the raw unwrapped phase in real-time measurements. A reference plane was placed at $z = 0$ for the phase–height conversion.

For the correlation of speckle images, although a larger size of subimages will generally reduce errors, the computational time will increase rapidly at the same time. Thus, to reduce the time cost, the size of the subimages to conduct the image correlation was $7 \times 7$ pixels in our experiments. Then, to cope with the errors, the multiple-correlation-peak correction algorithm was followed. The size of the neighborhood was set as $9 \times 9$ pixels.

### A. Accuracy Evaluation

First we tested the accuracy of the method by comparing it with the three-step PSP. The high frequency of the fringes of PSP is 100 cycles within the projection width. To unambiguously and correctly unwrap the high-frequency phase, a three-frequency phase unwrapping method was employed with other fringes of frequencies of 1 and 10 cycles across the width of 608 pixels. Here we measured a plane moving on the electric control translation stage with equal steps of 10 mm. The result is shown in Fig. 9. Figures 9(a) and 9(b) illustrate the average absolute error and the root-mean-square (RMS) error of the two methods. It can be seen that the accuracy of the proposed method is very close to that of the three-step phase-shifting method; only its RMS error is slightly higher than its counterpart. But this still meets the precision requirement for dynamic scene measurements. Besides, the proposed method greatly reduces the required number of patterns. Only two patterns are used in our method, which indicates the measuring speed could be improved by 77.8% compared with the traditional PSP method where nine frames are employed.

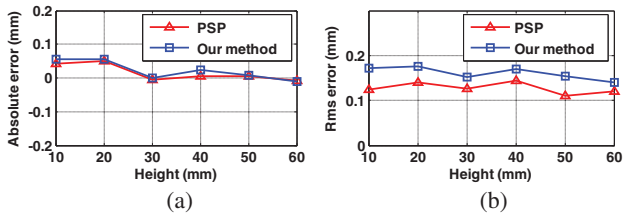


**Fig. 9.** Comparison between our method and PSP. (a) Average absolute error; (b) RMS error.

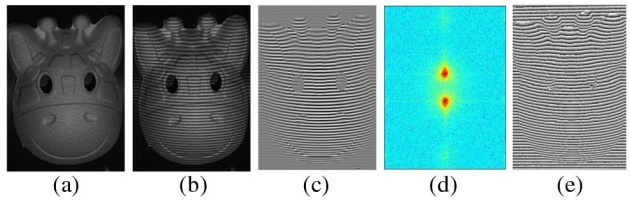


**Fig. 10.** Experimental images of the method measuring a static object. (a) Captured spekcle image; (b) captured speckle-embedded sinusoidal pattern; (c) resultant sinusoidal fringe after subtraction; (d) Fourier frequncy spectrum; (e) wrapped phase map solved by FTP.

### B. Static Object Measurement

Next we measured a cartoon face to show the system's performance handling a static scene. The experimental setup is shown in Fig. 8(b). Figures 10(a) and 10(b) are the captured speckle image and the speckle-embedded fringe image, respectively. After subtracting Fig. 10(a) from Fig. 10(b), a pure sinusoidal fringe image was obtained as shown in Fig. 10(c), and its spectrum is illustrated in Fig. 10(d). It can be seen that by appropriately adding the DC component, the fundamental frequency has been successfully eliminated. By FTP, the retrieved wrapped phase is shown in Fig. 10(e). The speckle image was then correlated with the reference speckle images saved in preparation to obtain a raw height distribution. Using the established relation of the height and the phase, a raw, unwrapped phase map was calculated, and by Eq. (10) the fringe order distribution was obtained. Figure 11(a) shows the solved fringe order without the multipeak correction method. The result can be seen to be pricky, indicating many fringe orders are incorrectly solved, which resulted from the large slope variation across the surface. Figure 11(d) shows the fringe order map calculated after the estimated height distribution was corrected by Eq. (13). As the correction algorithm refined the raw height distribution calculated by the correlation of speckle images, a more accurate position was obtained which can ensure a more precise unwrapped phase map to be solved when the refined height is substituted into the fitted polynomial. Therefore by Eq. (10), with the known wrapped phase acquired by FTP,

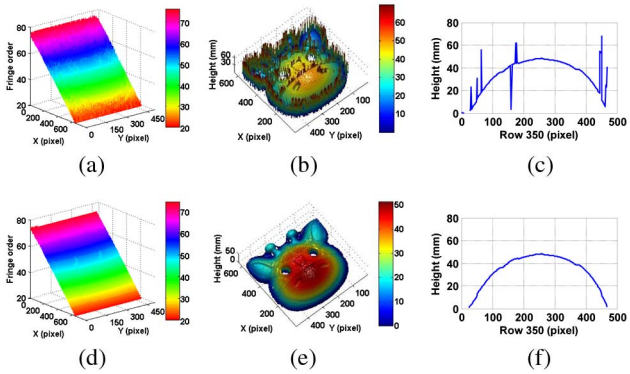


**Fig. 11.** Measurement results of the motionless object. (a)–(c) show the obtained fringe order, 3D reconstruction, and a plot of the 350th row of the 3D model before applying the height correction, respectively; (d)–(f) display the corresponding results after employing the correction.

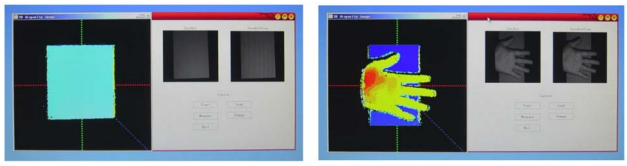

(a) (b)

**Fig. 12.** Snapshots of real-time measurements of dynamic scenes. (a) Measurement result of a shaking paper (see Visualization 1); (b) measurement result of a static box and a moving hand (see Visualization 2).

a more accurate fringe order map was computed. It can be seen that the former spiny fringe orders become smooth, indicating those erroneous fringe orders have been corrected successfully. The phase was then unwrapped and converted to the height. Figure 11(b) shows the reconstructed 3D result without the correction method, and Fig. 11(c) shows its cross section at the 350th row. It can be seen that there are lots of erroneous points with incorrect heights in the regions such as the nose and the eyes. After processing with the correction algorithm, the 3D reconstruction and the plot of its 350th row are illustrated in Fig. 11(e) and Fig. 11(f), respectively. It can be observed that those outliers have been corrected. The results show that accurate and efficient 3D reconstruction can be achieved with the presented two-pattern scheme.

### C. Real-Time Measurements of Dynamic Scenes

To show the real-time performance of our method, we first measured a shaking piece of paper. The measurement video and one of the frames are presented in Visualization 1 and Fig. 12(a), respectively. Pseudo color was used to represent the height information, where blue indicates a small height and red a large height from the reference plane $z = 0$. From the video it can be seen that the surface of the paper has been reconstructed correctly and the shaking process is retrieved smoothly.

Then we tested a static box and a human hand which is in front of the box and moving up and down, stretching and clenching. Visualization 2 and Fig. 12(b) show the measurement result. We find that the movements of the hand are clearly observed, and the phase map of these two isolated objects is correctly and unambiguously unwrapped, leading to a faithful 3D reconstruction of the scene. To see the time cost of the method, the processing time of the main procedures is listed in Table 1. With our experimental setup, the scene was measured at 21 FPS. We can find that the time-consuming parts are the correlation of speckle patterns and the correction of the height solved by the correlation. Thus if a GPU with more powerful computational capability is used, a higher measuring speed can be achieved. The experiments show that the proposed method can successfully implement 3D reconstructions of moving objects in real time.

**Table 1. Time Cost in the Real-Time Measurement**

| Procedure | Execution time |
|---|---|
| Images subtraction and FTP | 1 ms |
| Speckle patterns correlation | 26 ms |
| Correction of height solved by correlation | 17 ms |
| Fringe order calculation | 1 ms |
| Phase unwrapping | 1 ms |
| 3D reconstruction | 1 ms |
| Total | 47 ms |

## 6. CONCLUSION

A two-frame fringe projection technique using speckle-embedded patterns for real-time and unambiguous shape measurement has been presented. One of the frames is a digital speckle image that is used to eliminate the phase ambiguity, and the other frame is a composite pattern generated by synthesizing that speckle image with a sinusoidal fringe which is adopted to retrieve the phase. With this strategy and the developed fast data processing techniques based on a GPU, the method achieves real-time 3D reconstructions at 21 FPS. With the increasing need for fast, real-time 3-D measurement, we believe the proposed method will show great potential in a variety of applications.

However, it is worth mentioning that the accuracy of the method would depend on the result of the speckle image correlation since the phase unwrapping is conducted according to the height indicated by the maximal correlation value. Although the correction algorithm can be employed to improve the precision of the estimated height, for some surfaces of very complex shape, especially with too large slope or disturbed by partial discrete shadowing, the developed approach may perform unstably as the correlation between the captured speckle image and referenced ones would be very low. This will lead to difficulty in the estimation of the true peak of the correlation curve. In the future we will do our best to improve the method in this direction.

**Funding.** Fundamental Research Funds for the Central Universities (30915011318); Nanjing University of Science and Technology; Open Research Fund of Jiangsu Key Laboratory of Spectral Imaging & Intelligent Sense (3092014012200417).

## REFERENCES

1. F. Chen, G. M. Brown, and M. Song, "Overview of three-dimensional shape measurement using optical methods," Opt. Eng. **39**, 10–22 (2000).
2. S. S. Gorthi and P. Rastogi, "Fringe projection techniques: whither we are?" Opt. Lasers Eng. **48**, 133–140 (2010).
3. D. Murray and J. Little, "Using real-time stereo vision for mobile robot navigation," Auton. Robots **8**, 161–171 (2000).
4. Z. Wang, D. A. Nguyen, and J. C. Barnes, "Some practical considerations in fringe projection profilometry," Opt. Lasers Eng. **48**, 218–225 (2010).
5. Y. Cui, S. Schuon, D. Chan, S. Thrun, and C. Theobalt, "3D shape scanning with a time-of-flight camera," in *IEEE Conference on Computer Vision and Pattern Recognition (CVPR)* (IEEE, 2010), pp. 1173–1180.
6. H. Takasaki, "Moiré topography," Appl. Opt. **9**, 1467–1472 (1970).
7. S. Feng, Q. Chen, C. Zuo, J. Sun, and S. L. Yu, "High-speed real-time 3-D coordinates measurement based on fringe projection profilometry considering camera lens distortion," Opt. Commun. **329**, 44–56 (2014).
8. P. S. Huang, C. Zhang, and F.-P. Chiang, "High-speed 3-D shape measurement based on digital fringe projection," Opt. Eng. **42**, 163–168 (2003).

9. L. Huang, C. S. Ng, and A. K. Asundi, "Dynamic three-dimensional sensing for specular surface with monoscopic fringe reflectometry," Opt. Express **19**, 12809–12814 (2011).
10. Z. Zhang, C. E. Towers, and D. P. Towers, "Time efficient color fringe projection system for 3D shape and color using optimum 3-frequency selection," Opt. Express **14**, 6444–6455 (2006).
11. S. Feng, Q. Chen, C. Zuo, R. Li, G. Shen, and F. Feng, "Automatic identification and removal of outliers for high-speed fringe projection profilometry," Opt. Eng. **52**, 013605 (2013).
12. S. Zhang, "Recent progresses on real-time 3D shape measurement using digital fringe projection techniques," Opt. Lasers Eng. **48**, 149–158 (2010).
13. X. Su and Q. Zhang, "Dynamic 3-D shape measurement method: a review," Opt. Lasers Eng. **48**, 191–204 (2010).
14. T. R. Judge and P. J. Bryanston-Cross, "A review of phase unwrapping techniques in fringe analysis," Opt. Lasers Eng. **21**, 199–239 (1994).
15. J. M. Huntley and H. O. Saldner, "Shape measurement by temporal phase unwrapping and spatial light modulator-based fringe projector," Proc. SPIE **3100**, 185–192 (1997).
16. P. S. Huang and S. Zhang, "Fast three-step phase-shifting algorithm," Appl. Opt. **45**, 5086–5091 (2006).
17. M. Takeda and K. Mutoh, "Fourier transform profilometry for the automatic measurement of 3-D object shapes," Appl. Opt. **22**, 3977–3982 (1983).
18. X. Su and W. Chen, "Fourier transform profilometry: a review," Opt. Lasers Eng. **35**, 263–284 (2001).
19. Q. Zhang and X. Su, "High-speed optical measurement for the drumhead vibration," Opt. Express **13**, 3110–3116 (2005).
20. Q. Zhang, X. Su, Y. Cao, Y. Li, L. Xiang, and W. Chen, "Optical 3-D shape and deformation measurement of rotating blades using stroboscopic structured illumination," Opt. Eng. **44**, 113601 (2005).
21. L. Guo, X. Su, and J. Li, "Improved Fourier transform profilometry for the automatic measurement of 3D object shapes," Opt. Eng. **29**, 1439–1444 (1990).
22. J. M. Huntley and H. Saldner, "Temporal phase-unwrapping algorithm for automated interferogram analysis," Appl. Opt. **32**, 3047–3052 (1993).
23. C. Towers, D. Towers, and J. Jones, "Optimum frequency selection in multifrequency interferometry," Opt. Lett. **28**, 887–889 (2003).
24. K. Creath, "Step height measurement using two-wavelength phase-shifting interferometry," Appl. Opt. **26**, 2810–2816 (1987).
25. Y. Ding, J. Xi, Y. Yu, and J. Chicharo, "Recovering the absolute phase maps of two fringe patterns with selected frequencies," Opt. Lett. **36**, 2518–2520 (2011).
26. C. Towers, D. Towers, and J. Jones, "Time efficient Chinese remainder theorem algorithm for full-field fringe phase analysis in multi-wavelength interferometry," Opt. Express **12**, 1136–1143 (2004).
27. J. Li, L. G. Hassebrook, and C. Guan, "Optimized two-frequency phase-measuring-profilometry light-sensor temporal-noise sensitivity," J. Opt. Soc. Am. A **20**, 106–115 (2003).
28. C. Zuo, Q. Chen, G. Gu, S. Feng, and F. Feng, "High-speed three-dimensional profilometry for multiple objects with complex shapes," Opt. Express **20**, 19493–19510 (2012).
29. Z. H. Zhang, "Review of single-shot 3D shape measurement by phase calculation-based fringe projection techniques," Opt. Lasers Eng. **50**, 1097–1106 (2012).
30. Y. Wang and S. Zhang, "Superfast multifrequency phase-shifting technique with optimal pulse width modulation," Opt. Express **19**, 5149–5155 (2011).
31. K. Liu, Y. Wang, D. L. Lau, Q. Hao, and L. G. Hassebrook, "Dual-frequency pattern scheme for high-speed 3-D shape measurement," Opt. Express **18**, 5229–5244 (2010).
32. S. Lei and S. Zhang, "Flexible 3-D shape measurement using projector defocusing," Opt. Lett. **34**, 3080–3082 (2009).
33. Y. Wang and S. Zhang, "Optimal pulse width modulation for sinusoidal fringe generation with projector defocusing," Opt. Lett. **35**, 4121–4123 (2010).
34. C. Zuo, Q. Chen, G. Gu, S. Feng, F. Feng, R. Li, and G. Shen, "High-speed three-dimensional shape measurement for dynamic scenes using bi-frequency tripolar pulse-width-modulation fringe projection," Opt. Lasers Eng. **51**, 953–960 (2013).
35. Y. Zhang, Z. Xiong, and F. Wu, "Unambiguous 3D measurement from speckle-embedded fringe," Appl. Opt. **52**, 7797–7805 (2013).
36. S. Zhang, D. Royer, and S.-T. Yau, "GPU-assisted high-resolution, real-time 3-D shape measurement," Opt. Express **14**, 9120–9129 (2006).
37. H. Nguyen, D. Nguyen, Z. Wang, H. Kieu, and M. Le, "Real-time, high-accuracy 3D imaging and shape measurement," Appl. Opt. **54**, A9–A17 (2015).
38. H. Dai and X. Su, "Shape measurement by digital speckle temporal sequence correlation with digital light projector," Opt. Eng. **40**, 793–800 (2001).
39. W. Li, X. Su, and Z. Liu, "Large-scale three-dimensional object measurement: a practical coordinate mapping and image data-patching method," Appl. Opt. **40**, 3326–3333 (2001).